Wind Direction and Magnitude Determination Using Hall Effect-Based Rotary Encoders On High-Altitude Balloons

Maxim Somov[a], Sujay Venuganti[a]

Abstract

During the ascent stage of a high-altitude balloon flight, it is critical to know the local atmospheric conditions around the balloon. This paper explores the feasibility of using Hall effect-based rotary encoders in conjunction with accelerometric and barometric data to determine both wind direction and speed in the XYZ coordinate frame. The paper also addresses issues and challenges that arise when manufacturing and implementing the technology. Neodymium magnets were used to construct an anemometer and a wind vane which were then both mounted radially on either side of a payload structure. The anemometer and wind vane were both 3D printed and a contactless stem was used to position the magnets above a rotary encoder. The changes in magnetic field strength were then recorded throughout the flight and post-processed to create XY plane wind speed and direction. Accelerometer data was also used to offset rotational motion caused by the flight string. Using an accelerometer and barometer, the wind speed in the z-axis was then also estimated to predict the incoming total XYZ coordinate frame wind vectors. Test flights with this payload were conducted in both daylight conditions as well as in the 2024 total solar eclipse. Initial information related to this research suggests that although rotary encoders are easy to implement, limitations related to the real-time processing of data may pose difficulties in correctly analyzing the data.

Wind Speed | Wind Direction | Anemometer | Wind Vane | 3D Printed | Rotation Correction | Hall Effect-Based Rotary Encoders

1. Introduction

The first part of this study experimentally determines the magnitude of local wind vectors in the XY plane using a custom-built anemometer and wind vane. A rotation de-coupling algorithm is applied to know the exact position of the wind vector relative to the inertial coordinate system. The next part of this study uses an environmental sensor to determine the vertical velocity of a payload during the ascent stage of a high-altitude balloon flight. Numerical differentiation is employed to determine the z-axis wind gusts. Lastly, this study explores the feasibility of implementing 3D-printed anemometers and wind vanes to high-altitude balloon flights. Possible limitations related to this technology are then discussed.

To achieve the objectives mentioned, the team constructed a custom payload structure. The payload structure was 3D printed and used consumer-grade electronics and sensors. An anemometer and wind vane were both mounted on opposite corners of a payload structure and configured to record the wind speed and wind direction during the ascent stage of a high-altitude balloon flight. The flight string (nylon rope) was run through the center of the structure in an attempt to minimize pitch and roll. An accelerometer was then mounted near the center of

[a]Undergraduate student, Virginia Polytechnic Institute and State University, Blacksburg, VA

rotation and calibrated. As the payload experienced rotational motion, the accelerometer would detect the angle through which the rotation occurred and subtract the structural motion due to wind from the angle the wind vane detected. This, in essence, de-coupled the rotational motion of the payload structure from the true angle of the wind vector. To collect data, this payload was flown two times in 2024 with the High-Altitude Ballooning at Virginia Tech (HAB@VT) design team. The first flight occurred on February 24, 2024, and recorded roughly 31 minutes of data. The next flight opportunity occurred on April 8, 2024, during the total solar eclipse and provided about 51 minutes of data for the team.

To record the local XY plane wind direction and magnitude, the team built an in-house anemometer and wind vane system. At its core, these were 3D-printed components mounted onto sealed radial ball bearings. A diametrically magnetized ring magnet was then attached to the stem of the anemometer and wind vane structure. An AS5600 magnetic encoder was then positioned near the magnet and recorded the changes in magnetic field strength as the diametric magnet rotated. This data was then converted into rotations per minute (RPM) for the anemometer and raw angle for the wind vane. A calibrated accelerometer was then used to determine the rotation of the structure and a de-coupling algorithm was applied to the wind vane to determine true wind direction. A BME280 environmental sensor was then used to determine the changes in pressure during the flight. The pressure was then converted to altitude and the z-axis velocity was determined through numerical differentiation. Finally, the feasibility of implementing 3D-printed anemometers and wind vanes is examined at the end of the paper along with a brief discussion of what was successful and what was not. The theoretical background information related to this study is found in the succeeding section:

1.1. Hall Effect-Based Rotary Encoder Wind Speed

The first technology the team used was Hall effect-based rotary encoders. These are essentially electronic chips that detect and return the local magnetic field strength. Figure 1 shows a simple outline of how a hall-effect based rotary encoder works [1]. By attaching a magnet to a rotating shaft and applying a constant angular velocity, the chip would return a sinusoidal signal proportional to the magnet's position. By determining the change in time between subsequent data points, the instantaneous angular velocity can then be determined. This is exactly what was done to determine the RPM (revolutions per minute) of the anemometer. After the RPM was computed, the linear equation estimate seen in (1) was applied. This function was determined experimentally during ground testing and returns the estimated velocity in meters per second for a given RPM. To do this, a handheld anemometer was used alongside a blower fan. As the fan speed was varied, the anemometer wind speed was recorded with the corresponding anemometer RPM. A linear regression model was then applied to the recorded values. Note that the function includes a minimum value for which the anemometer can detect wind speed. The team determined that below about 3 meters per second, the anemometer was not sensitive enough to detect wind speed. In the equation, y(x) is the velocity in m/s for a given instantaneous RPM value x.

$$y(x) = 0.174x + 3.065 \tag{1}$$
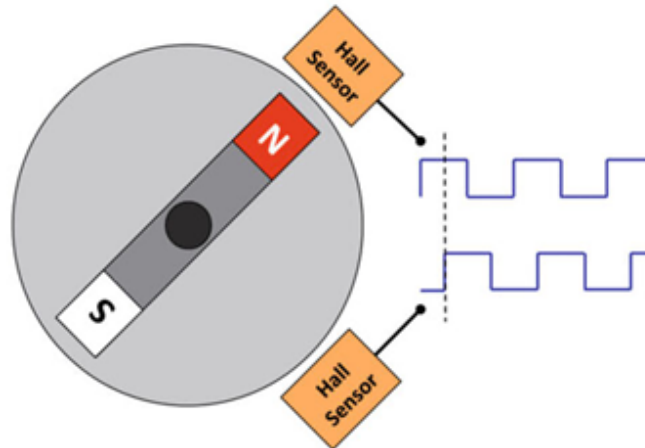
Fig. 1. Diagram showing how a Hall effect-based rotary encoder works taken from [1]. Note that the real sensor exerts a sinusoidal-like wave while the diagram depicts a square wave.

### 1.2. Hall Effect-Based Rotary Encoder Wind Direction and Rotation Compensation Algorithm

Wind direction was also determined using a very similar method to that described earlier. However, because wind direction is analogous to position in the linear sense, the time increment was not necessary and the raw angle can be read from the encoder as seen in Figure 1. Because the payload structure is constantly rotating due to pressure gradients (wind) in the atmosphere, the team opted to introduce a rotation compensation algorithm. This algorithm was only applied to the wind vane. This system consisted of a BNO055 9-axis inertial measurement unit that internally fused accelerometer, gyroscope, and magnetometer data together to determine the payload structure relative to the inertial reference frame. The inertial frame, in this study, is defined as a set of unit vectors in which the x-axis $(\hat{i})$ points towards the magnetic east, the y-axis $(\hat{j})$ points towards the magnetic north, and the z-axis $(\hat{k})$ completes the right-hand coordinate system rule. As the payload structure rotated, the angle detected between the wind vane and the payload structure could be subtracted/added to determine the true wind direction. Figure 2 shows the default configuration where the wind vane is pointing towards the inertial x-axis (east). The recorded angle in this configuration is 0 degrees, meaning the wind vector is going purely eastward. Figure 3 then depicts a wind change where the wind vane is now at 45 degrees. Figure 4 then shows a rotation of the payload structure of 20 degrees relative to the east. The wind vane still remains at 45 degrees relative to the inertial frame. However, the angle recorded from the payload structure (i.e., local frame) now says 25 degrees because the structure has moved, as seen in Figure 5.
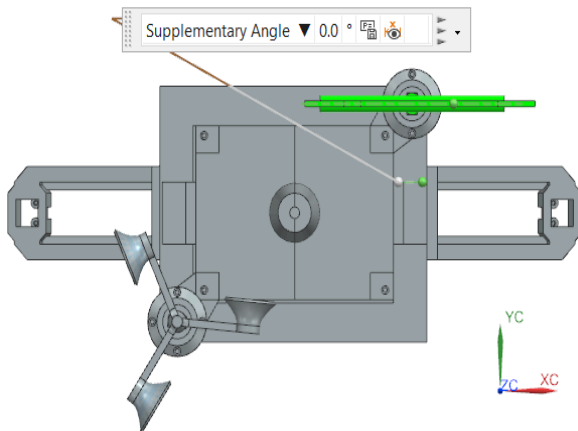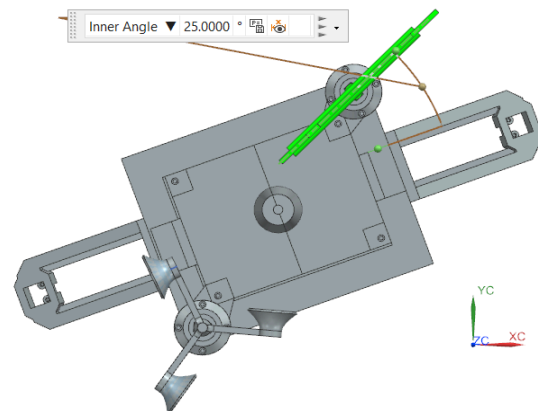
Fig. 2. Picture showing the wind vane aligned with the payload structure with 0 degrees offset from the inertial XC axis.
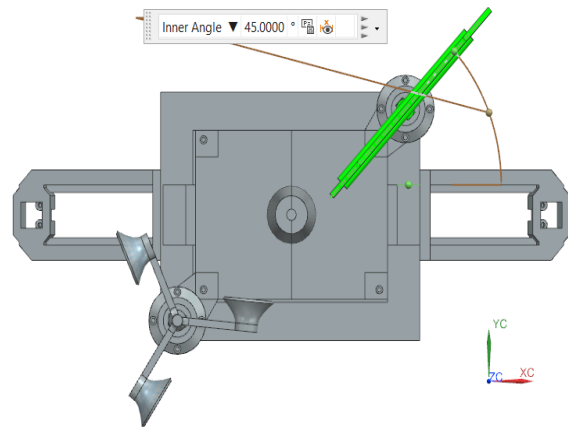
Fig. 3. Picture showing the wind vane at a 45-degree offset from the inertial XC axis.
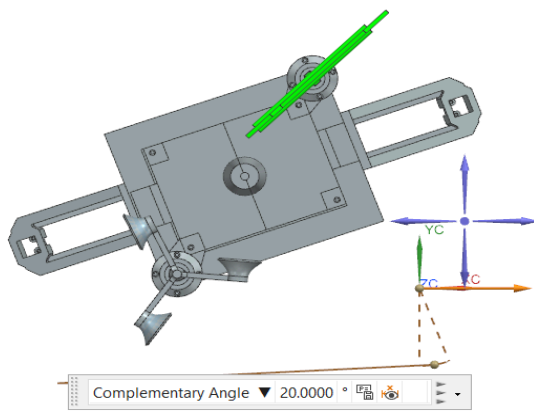
Fig. 4. Picture showing a 20-degree offset for the payload structure relative to the XC axis.

Fig. 5. Picture showing the new relative wind vane angle of 25 degrees relative to the payload structure. The angle relative to the inertial XC axis is still 45 degrees.

As a result, the team implemented a rotation compensation algorithm onto the main payload computer to compensate for this rotation in real-time. At its core, the program recorded the quaternions from the BNO055 IMU and then converted the values to degrees to find the payload position relative to the east-axis vector. Then, the program would record the wind-vane angle and subtract/add the values to determine the true wind direction. Because the wind-vane detects the change in wind direction relative to the drifting payload structure, the wind direction and magnitude in this study are differential winds relative to the balloon's overall drift motion.

1.3. Z-Axis Velocity and 3D Magnitude

Another important aspect of the payload was to determine the z-axis velocity. This was done by utilizing a BME280 environmental sensor. The sensor would record the ambient pressure using

the built-in barometric chip. This data from the chip would then be analyzed by BME280 and sent to the main computer in the form of an altitude in meters. Knowing the elapsed time between measurements, (2) can then be applied to the dataset via numerical differentiation. This calculation, in turn, would give the instantaneous velocity in the z-axis at a given time. In this equation, the j value is the change in time between data points (1 second), whereas f(i+j) and f(i) are the positions in meters at times $i + j$ and i. The resulting velocity would then be given in m/s.

$$z = \frac{f(i+j) - f(i)}{j} \tag{2}$$

To calculate the true 3D velocity vector, (3) can be used to determine the x-axis (west-east) component of velocity by knowing the east-north (XY) plane magnitude and angle from the anemometer and wind vane.

$$x = v_{anemometer} cos(\theta_{wind\ vane}) \tag{3}$$

Then, (4) is used to determine the y-axis (north-south) component of velocity.

$$y = v_{anemometer} sin(\theta_{wind\ vane}) \tag{4}$$

Finally, (5) is used to calculate the magnitude of the velocity vector in 3D space by knowing all of the vector components at a given time.

$$|V| = \sqrt{x^2 + y^2 + z^2} \tag{5}$$
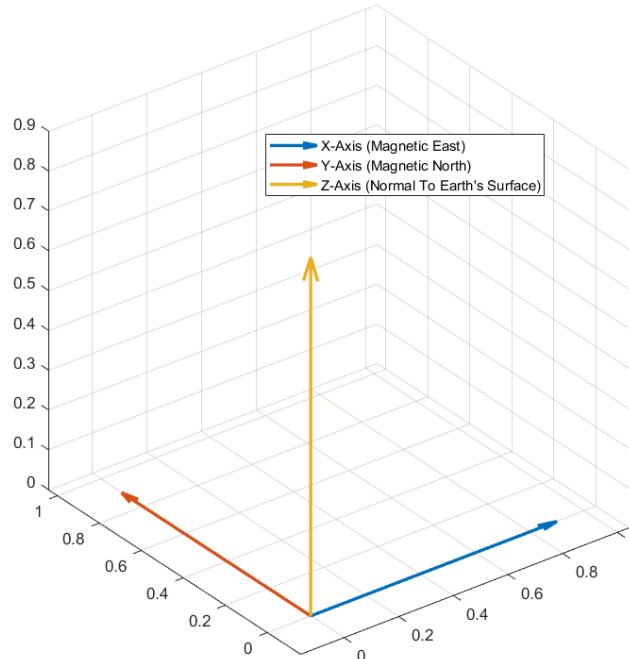
Fig. 6. 3D Visualization of the coordinate system used to compute the wind-direction magnitude as shown in (3-5).

1.4. Report Overview

The report is organized in the following structure. A brief theoretical background relating to Hall effect-based rotary encoders as well as how the team utilized this technology to build a custom payload structure is introduced at the beginning. The electronics and payload structure used to develop the payload and record data are then detailed. An overview of the data the team recorded is presented, relevant observations and remarks are made, and conclusions are made with an overview of the deductions drawn from the data.

2. Structure and Electronics

2.1. Payload Structure

The payload structure used in this paper is a custom-built 3D-printed superstructure with attachment points for various electronics and sensors. The payload was 3D modeled using Siemens NX CAD software and manufactured, assembled, and tested at the HAB@VT laboratory. All structures were manufactured using polylactic acid (PLA) plastic on an Ender-3 3D printer. The center of the structure also has a hole for the flight string. The flight string consists of a nylon rope that holds payloads together during the flight. Knots were made on either end of the payload structure to prevent it from sliding.

Figure 7 shows a full 3D render of the payload. On the roof of the structure, there are two mounting points located on opposite sides of one another for the anemometer and wind vane. Figure 8 shows a top-down view of the structure with the anemometer and wind vane mounted. The anemometer and wind vane were also designed and fabricated by the team and are shown in Figures 9 and 10. A shaft link was then used to mount the anemometer and wind vane to a set of 608-2RS ball bearings and the ball bearings were mounted into a coupler section which was attached to the mounting points. Figures 11 and 12 show an exploded view of the anemometer

and wind vane during assembly, respectively. Figure 13 shows the ball bearing and magnet used with the AS5600 magnetic encoder. Finally, after assembly was complete, the payload was placed in a 6.5-inch by 8-inch box with a uniform wall thickness of about 1 inch for improved heat retention.
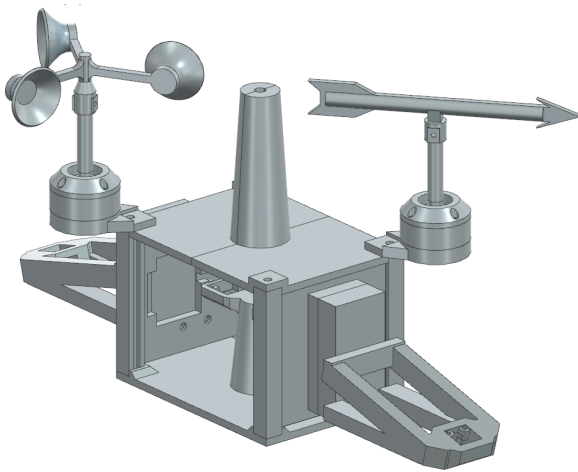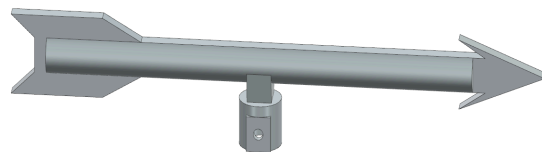

Fig. 7. Fully 3D render of payload structure.
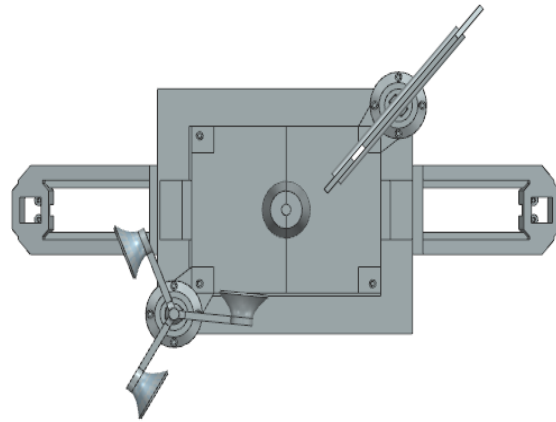
Fig. 8. Top-down view of the 3D rendered payload structure.
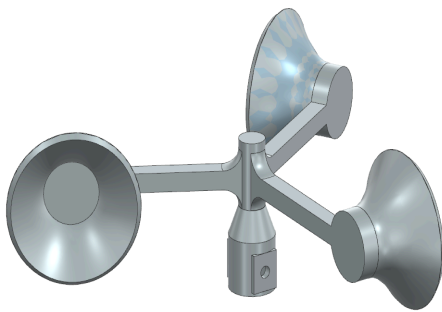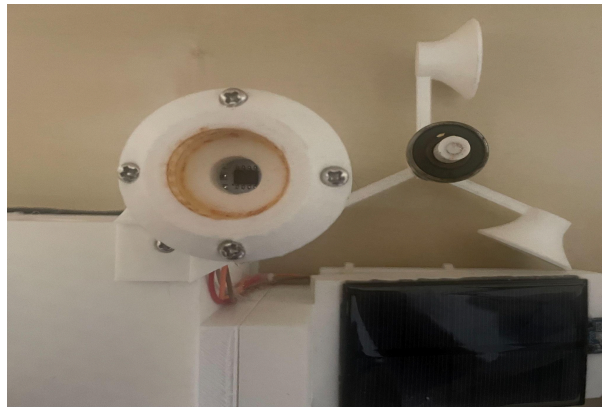

Fig. 9. 3D render of the anemometer.

Fig. 10. 3D render of the wind vane.

Fig. 11. Exploded view of how the anemometer is assembled.

Fig. 12. Exploded view of how the wind vane is assembled.

Fig. 13. Picture showing the mounting points for the anemometer. The AS5600 sensor is visible inside the mounting point. Next to the mounting point, on the table, is the anemometer structure with a ball bearing attached to the shaft. The end of the shaft has a diametric magnet attached.

Near the center of the payload are the BNO055 IMU and BME280 mounting points. These sensors are located near the center of gravity of the structure and have a pressure tap next to them to allow for pressure equalization. This location for the sensors was also chosen as it is furthest away from other sensors that may interfere with the data (such as the magnetometer on the IMU). Figure 14 shows the structure used to mount the sensors.
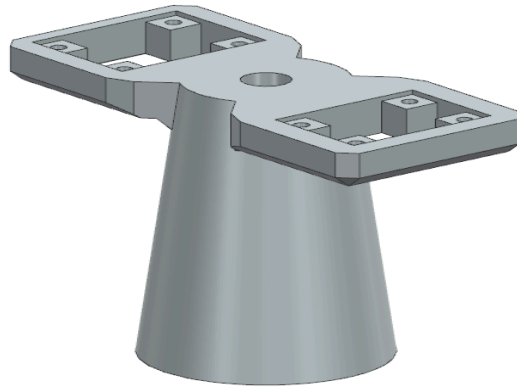
Fig. 14. Pictured is the mounting system for the BME280 and BNO055. The nylon flight string to hold the payloads runs through the center of the structure.

2.2. Main Payload Electronics

To record the changes in the magnetic field an AS5600 magnetic encoder (AS5600 encoder is analogous to an AS5600 sensor) was utilized. This sensor is 12-bit and is manufactured by Teyleten Robot. According to the manufacturer, this results in "4096 positions per round" and has "no rotation angle limitation" [2]. Provided diametric magnets that came with the sensor were also used. The sensor uses the I2C communication protocol to communicate with the main onboard computer and the AS5600 Arduino C library by Robert Tillaart was used [3]. To prevent aliasing problems related to the sampling rate, the team chose a wait time of .5ms (2kHz) for the anemometer and 20ms (50Hz) for the wind vane. The wind vane sampling frequency was limited by the BNO055 IMU because the two sensors worked in conjunction.

The next important sensor the team used was the BNO055 9-axis IMU manufactured by Adafruit. Once calibrated, the team used the internal fusion algorithm to obtain the quaternion angles (in the XYZ inertial frame) of the sensor. The accelerometer has acceleration range of ±2g/±4g/±8g/±16g and a low-pass filter bandwidth of 1kHz - <8Hz, the gyroscope has a range of ±125°/s to ±2000°/s with low-pass filter bandwidth of 523Hz - 12Hz, and a magnetometer of range ±1300µT (x-, y-axis); ±2500µT (z-axis) with a resolution of ~0.3µT [4]. The absolute orientation (quaternion) can be obtained at 100Hz while the magnetic field strength vector can be obtained at 20Hz [5]. As a result, the team chose to use the 20Hz option to allow for magnetometer synchronization which resulted in a delay time of 20ms (50Hz). Similar to the AS5600 magnetic encoder, this sensor also uses the I2C communication protocol. Finally, there is the BME280 sensor. This sensor is used to record the altitude from barometric pressure every 20ms and has an "±1 meter or better accuracy" [6].

2.3. Additional Electronics

To control all the sensors, an Adafruit Feather M0 Adalogger was used as the primary flight computer. This chip not only had a micro SD card breakout that the team utilized for data logging but it also had 256KB of FLASH which was crucial when using multiple open-source libraries to code the sensors [7]. In terms of software, the team utilized Arduino C to write all the functions used to control the sensors. The Feather M0 was configured to save data every 1 second after initial calibration was completed. Because multiple AS5600s were used, the team

also implemented a HiLetgo TCA9548A I2C multiplexer. This device allowed multiple sensors to be run that have the same I2C address. Apart from the 3 main sensors mentioned in the preceding paragraph, the team also mounted 2 solar panels (non-power generative) and 4 other sensors related to another experimental study on the payload structure. To power the electronics, a 500mAh, 3.7V Lithium ion battery was used on the February 24 flight and a 2000mAh, 3.7V Lithium ion battery was used for the April 8 flight. Connections between the electronics were made using 22 AWG wires alongside ELEGOO jumper ribbon cables. After all electronics and structural components were secured inside the payload structure, the payload had a mass of 860g on the February flight and 968g on the April flight.

2.4. Uncertainty and Issues

Although interpreting data at face value is often tempting, it is important to understand the uncertainties and issues associated with it. To start, there are the primary uncertainties associated with the main sensors. As briefly mentioned in the previous section, this includes the following values: the 12-bit limit on the AS5600 (no known range), 20Hz on the BNO055 (more precise values above), and ±1 meter on the BME280. Because the discussed payload was also custom-built, there are non-measurable uncertainties that the team was not able to measure, such as the anemometer efficiency, optimal wind vane design, and non-rotational pitch or roll. The first issue the team faced was the temperature within the payload. Looking at Figure 6, it is shown that the AS5600 sensors were mounted on the outside of the main structure near the anemometer and wind vane. As a result, these sensors experienced temperatures outside of their assumed operational range. Consequently, the team believes this low temperature caused issues with the recorded data. Another issue the team experienced was the pitch and roll of the payload structure. Because the BNO055 algorithm considers only the rotational motion of the structure, the other effects on the wind vane are not considered. This can be a big oversight in certain events, such as when a high-altitude balloon enters the jet stream or when turbulence causes distributions below the balloon. Altogether, the team believes that these uncertainties need to be addressed and considered when viewing and analyzing the data in this report.

Another possible issue worth discussing is the ambient atmospheric pressure changes as the payload structure ascends during the mission. The anemometer is a pressure-sensitive device, and, as such, is affected by pressure fluctuations at different altitudes (particles provide a force on the device). Additionally, the barometric formula, often used to estimate atmospheric pressure, exponentially decays as a function of height - hence implying that accurate readings may decrease with altitude. Unfortunately, the team did not conduct testing in low-pressure environments and cannot adequately quantify the effects of ambient pressure decrease or produce a presumably functioning range of the anemometer. This issue is worth keeping in mind when viewing the anemometer data in the following sections, especially at higher altitudes.

3. Results and Discussion

3.1. February Flight RPM and Wind Direction

The first flight occurred on February 24. The payload was launched from Kentland Experimental Aerial Systems (KEAS) Laboratory in Blacksburg, Virginia at about 9:30 am EST on a Kaymont 1600g. The payload was secured about 50 feet below the balloon alongside 6 other payloads. The first data that is of interest for this analysis is the raw recorded RPM and angle from the anemometer and wind vane. Figure 15 shows the recorded RPM over the duration ascent stage while Figure 16 shows the recorded (and corrected) angle in degrees where 0 degrees

corresponds to magnetic east. The data is already pre-trimmed to include only the ascent stage of the flight. Looking at the raw data, it is very difficult to reach any conclusions. Additionally, it is also important to note that the RPM is negative at times. This simply means that the wind is blowing in the opposite direction (I.E, clockwise magnetic encoder rotation is positive while counter-clockwise is negative).
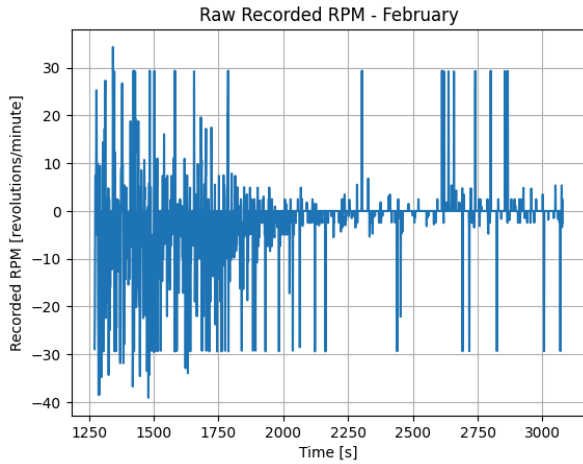

Fig. 15. Figure showing the recorded RPM by the anemometer during the February flight.
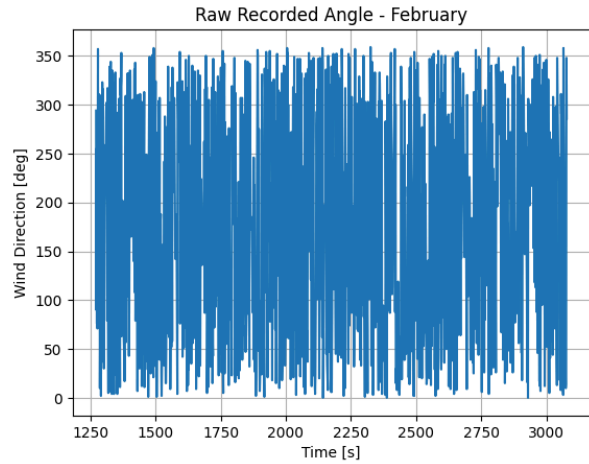
Fig. 16. Figure showing the recorded angle from the wind vane in degrees during the February flight.

To interpret the data in an easier way, another type of plot can be created: the polar plot. Figures 17 and 18 show the polar plots for the wind speed and wind direction on the east-north (XY) plane. Figure 17 was created by matching the instantaneous wind speed with the instantaneous recorded angle. Figure 18 was created in a similar manner except the duration of time is matched with the wind vane angle. Figures 19 and 20 are also included to show the path the balloon took during the February flight and the corresponding direction on the polar plot. It is also important to note that this dataset only captures about half the ascent stage due to battery problems. As a result, when compared to Figure 19, the data is valid only around the halfway point.
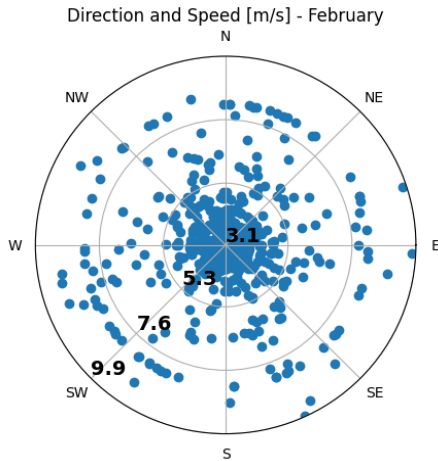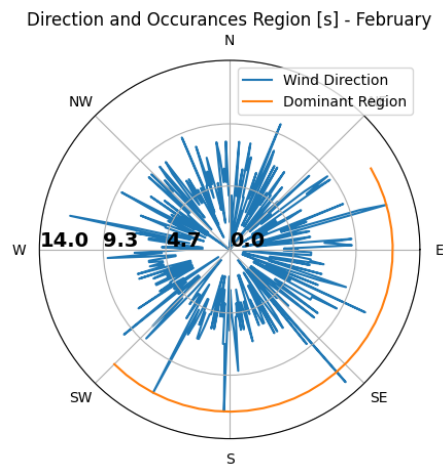
Fig. 17. Polar plot showing the wind speed during the February flight.
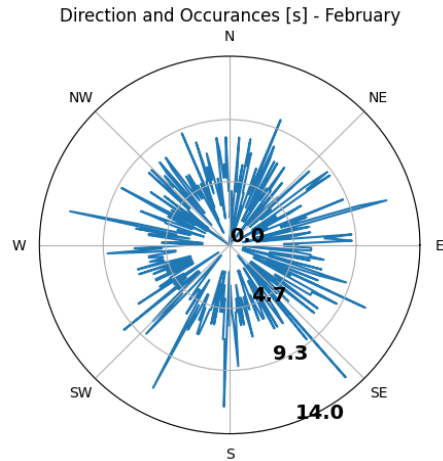
Fig. 18. Polar plot showing the wind direction and occurrences during the February flight.
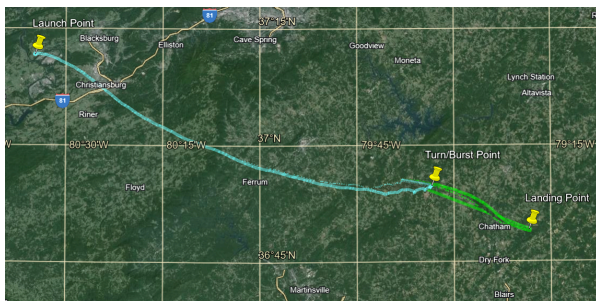

Fig. 19. Flight path for the February flight.

Fig. 20. Polar plot showing the wind direction with the dominant region in orange matching the February flight path.

Although the team believes the wind vane did an acceptable job at recording the wind direction angle, the anemometer, on the other hand, seems to become saturated at high RPMs as the balloon enters regions of high wind (such as the jet stream). The team believes that either the low temperature or low sampling rate is causing these problems. As such, the team generated Figure 21 which attempts to show the limitations of the anemometer. This figure also includes the recorded altitude shown as the black line and the reliable data region shown in green.
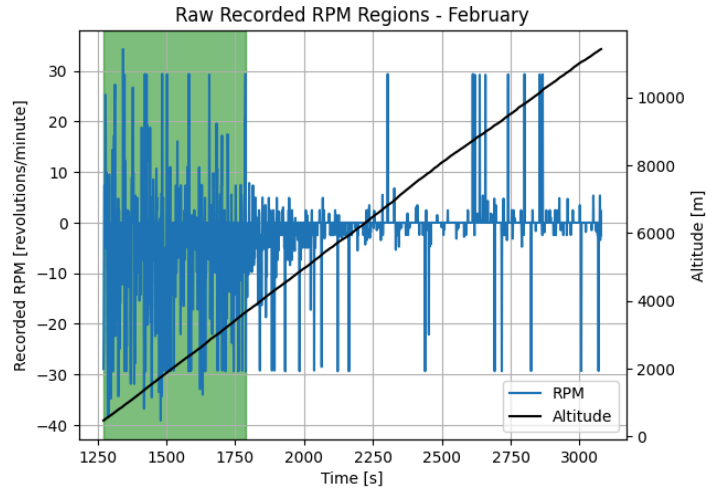
Fig. 21. Figure showing the estimated region where the anemometer exceeded its design limitations. The highlighted green section indicates the reliable data region.

3.2. February Flight Z-Axis Velocity and Total Magnitude

As discussed in the objectives of the study, another value of interest is the z-axis velocity. Figure 22 shows the raw z-axis velocity when applying numerical differentiation to the altitude data with (2). On the February flight, the team predicted a 7.7m/s average ascent velocity using computer modeling. As such, the instantaneous z-axis velocity can then be computed by subtracting the total z-axis velocity at an instant in time from the estimated average. Figure 23 depicts the instantaneous, scaled z-axis velocity during the flight.
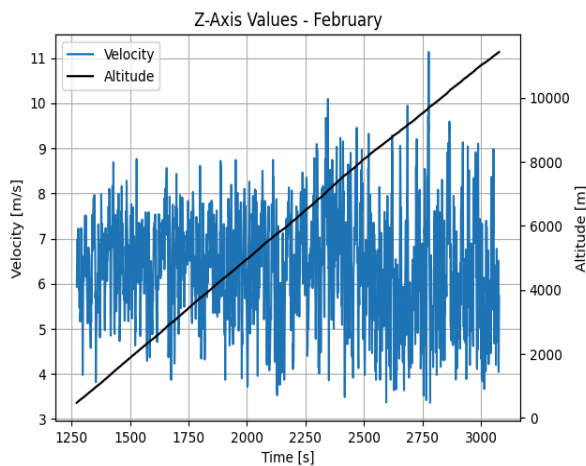
**Fig. 22.** Figure showing the vertical velocity during the February flight.
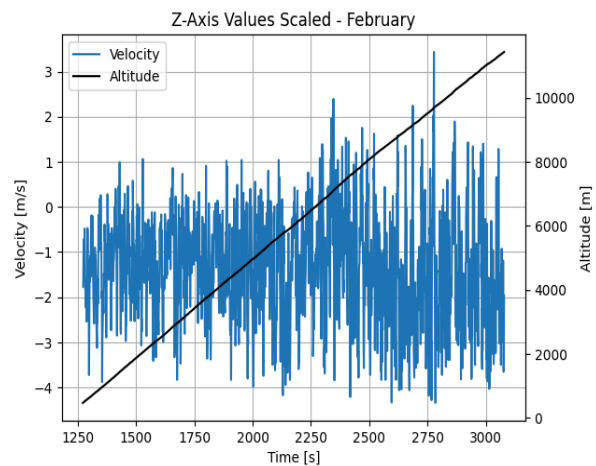
Fig. 23. Figure showing the real vertical velocity by accounting for the constant ascent rate during the February flight.

Equations (3), (4), and (5) can then all be used to determine the individual velocity vector components for a data point. Figure 24 shows the corresponding magnitude graph against time

while Figure 25 shows the reliable data region where the team believes the magnitude is most accurate.
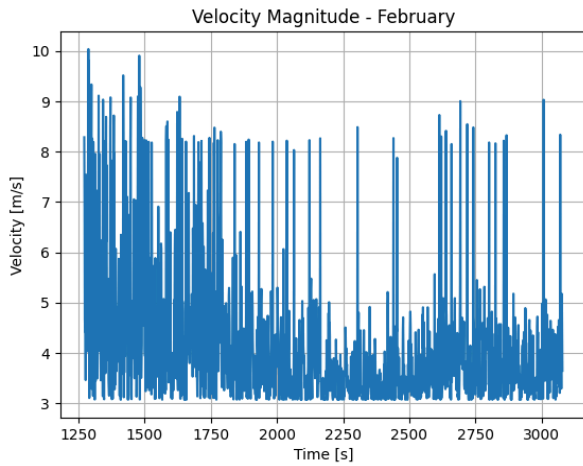
Fig. 24. Calculated wind magnitude when taking into account all 3 vector velocity components on the February flight.
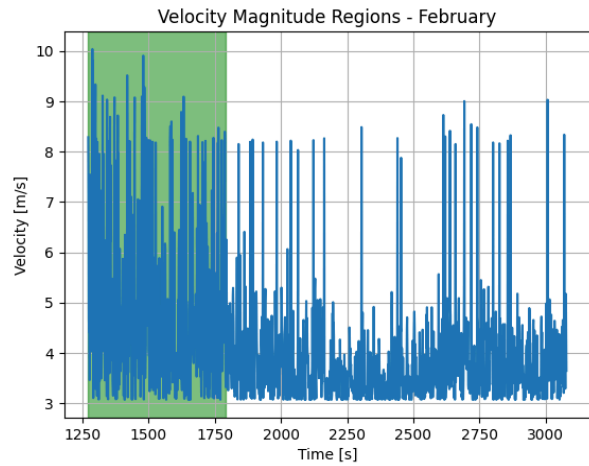

Fig. 25. Reliable data region where the team believes the calculated magnitude is most accurate (shaded green) for the February flight.

3.3. April Flight RPM and Wind Direction

The next flight opportunity occurred on April 8th from Thayer High School in Thayer, Missouri during the 2024 total solar eclipse. This launch occurred at about 12:30 pm CDT on a Kaymont 2000g balloon with 8 other payloads. The payload was secured about 80 feet from the balloon. For simplicity, the raw data is not shown and only the polar plots and flight path are provided in Figures 26-29. The plots, like the February flight, show that the wind vane successfully captured the flight wind direction. Unlike the February flight, this dataset also recorded the entire flight duration so the path in Figure 28 directly matches Figure 29 in terms of dataset duration.
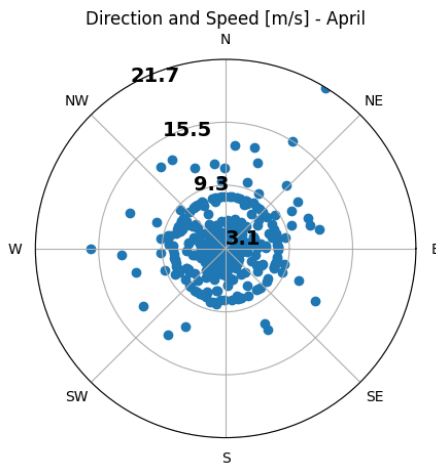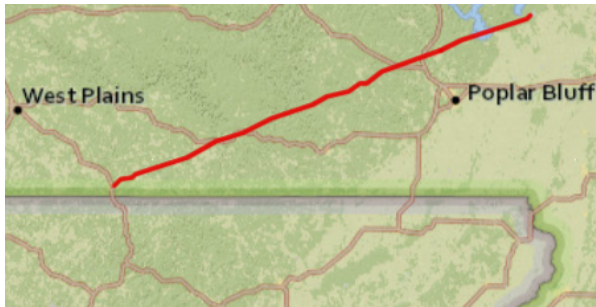

Fig. 26. Polar plot showing the wind speed during the April flight.
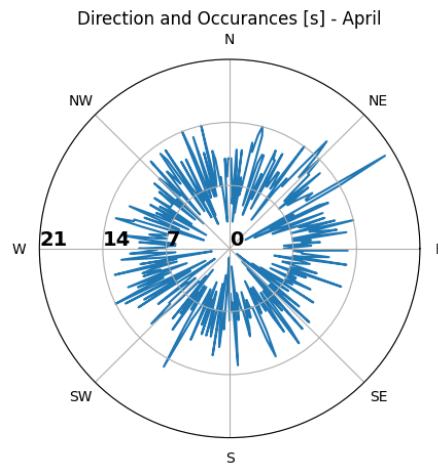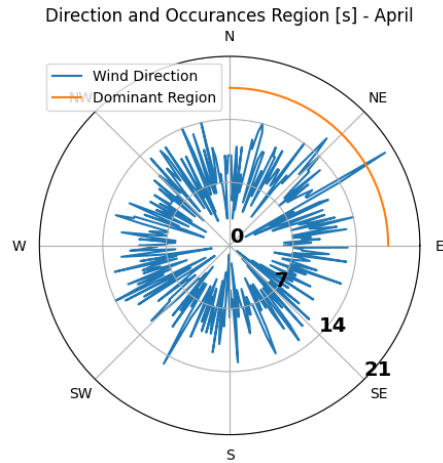

Fig. 27. Polar plot showing the wind direction and occurrences during the April flight.

Fig. 28. Flight path for the April flight shown in red. Arkansas state line shown in light gray below. Town names are also visible.

Fig. 29. Polar plot showing the wind direction with the dominant region in orange matching the April flight path.

### 3.4. April Flight Z-Axis Velocity and Total Magnitude

The z-axis velocity can also be determined as described earlier. Equation (2) is applied to the pressure values to generate Figure 30. During this flight, the team predicted a 6.2m/s average ascent velocity. As such, Figure 31 is also generated to show the pure instantaneous z-axis velocity change due to wind and gusts. One interesting thing that can be observed in Figure 31 is the oscillations toward the end of the flight. The team cannot adequately explain these oscillations as they may be a result of either atmospheric conditions or sensor issues. For reference, Figure 32 is included to show the entire z-axis velocity during the flight with the total eclipse marked in green.
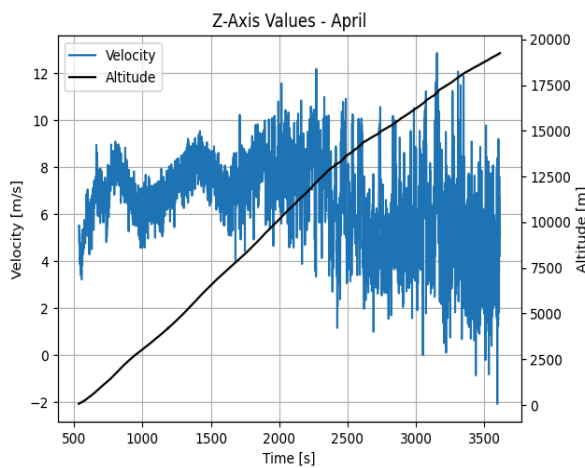
Fig. 30. Calculated wind magnitude when taking into account all 3 vector velocity components on the April flight.
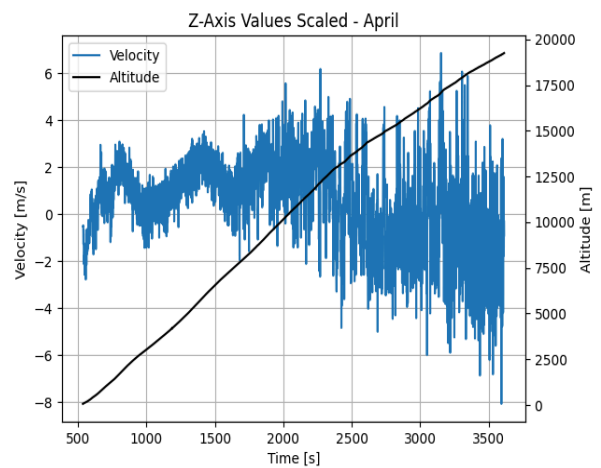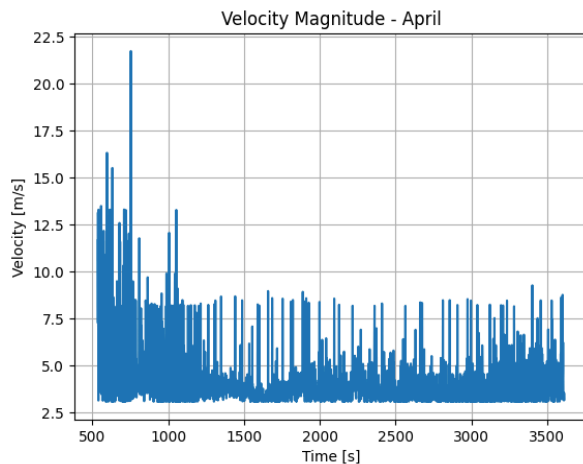
Fig. 31. Figure showing the real vertical velocity by accounting for the constant ascent rate during the April flight.
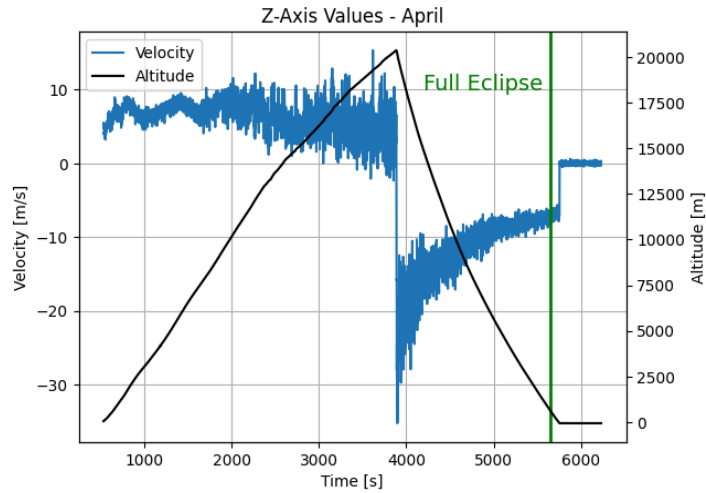
Fig. 32. Figure showing the entire vertical velocity during the April flight

Finally, the 3D velocity magnitude can once again be computed and shown in Figure 33. Figure 34, like last time, is also provided to show the reliable data region in which the anemometer was working before environmental effects reduced its recording ability, just like in the February flight.

Fig. 33. Figure showing the vertical velocity during the April flight.
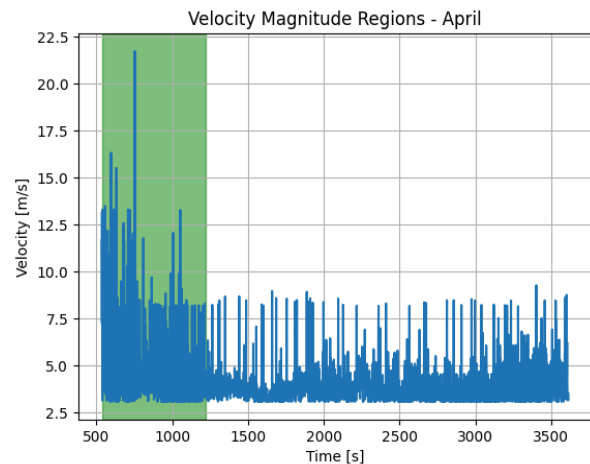
Fig. 34. Reliable data region where the team believes the calculated magnitude is most accurate (shaded green) for the April flight.

4. Conclusion

An experiment has been performed by members of the HAB@VT design team to determine how wind velocity and direction can be recorded during high-altitude balloon flights. The team utilized Hall effect-based magnetic encoders to create a custom anemometer and wind vane that was attached to a 3D-printed payload structure. The anemometer recorded the east-north (XY) wind magnitude while the wind vane recorded the corresponding direction. The team also

utilized a rotation-compensation algorithm alongside the wind vane to account for the yaw (rotational) motion of the structure. This algorithm did not account for the pitch or roll but provided the wind vector relative to an inertial reference frame. Finally, the team also utilized a BME280 to calculate the z-axis velocity by measuring the vertical distance traveled (due to barometric pressure changes) and dividing it by the corresponding time segment. Following the team's analysis of the datasets, the following conclusions were made.

Hall effect-based rotary encoders may be a viable device for measuring the wind direction in high-altitude balloon flights. However, pitch, yaw, and roll must all be accounted for as the structure travels through the air as they introduce motion not related to the wind. Additionally, although Hall effect-based rotary encoders do have promising potential for measuring wind speed, the team believes changes need to be made to the anemometer design and computing power. From the team's experience, the anemometers experienced saturation when the anemometer exceeded a certain RPM, the temperature dropped too low, and the sampling rate was too slow. This occurred on both test flights the team conducted and a re-design would be necessary to properly record data during the entire flight. Furthermore, preliminary data suggests that using a BME280 environmental sensor for z-axis velocity determination is possible. By differentiating the barometric altitude data, it is possible to estimate the vertical velocity of the high-altitude balloon during the ascent stage of the mission. Although this currently involves post-processing the data, the team believes this can be coded into the sensor itself. Finally, the team believes there is great potential in using 3D-printed components for various atmospheric wind-related measurements. In the team's experience, most failures resulted from the electronic components on board the payload. As such, the team believes there is great potential in creating custom, lightweight, measuring devices that can be easily mounted and integrated into high-altitude balloon payloads.

References

1   Avnet Staff, "How are magnetic rotary encoders used in industrial automation?," Avnet, https://www.avnet.com/wps/portal/us/resources/article/magnetic-rotary-encoders-in-industrial-automation/ (accessed May 17, 2024).
2   "Grove - 12-bit Magnetic Rotary Position Sensor / Encoder (AS5600)," https://www.mouser.com/pdfDocs/seeedstudio_com1.pdf (accessed May 17, 2024).
3   Rob Tillaart, "AS5600," GitHub, https://github.com/RobTillaart/AS5600 (accessed May 17, 2024).
4   Bosch Sensortec, "BNO055 Intelligent 9-axis absolute orientation sensor," Adafruit, https://cdn-shop.adafruit.com/datasheets/BST_BNO055_DS000_12.pdf.
5   Adafruit BNO055 Absolute Orientation Sensor. In Adafruit. Available: https://learn.adafruit.com/adafruit-bno055-absolute-orientation-sensor/overview
6   Adafruit BME280 I2C or SPI Temperature Humidity Pressure Sensor - STEMMA QT. In Adafruit. Available: https://www.adafruit.com/product/2652. (accessed May 17, 2024).
7   "Adafruit Feather M0 Adalogger," Adafruit, https://www.adafruit.com/product/2796 (accessed May 17, 2024).